Neural-Hidden-CRF: A Robust Weakly-Supervised Sequence Labeler

Zhijun Chen
SKLSDE Lab, Beihang University
Beijing, China
zhijunchen@buaa.edu.cn

Hailong Sun*
SKLSDE Lab, Beihang University
Beijing, China
sunhl@buaa.edu.cn

Wanhao Zhang
Institute for Network Sciences and
Cyberspace, Tsinghua University
Beijing, China
zwh22@mails.tsinghua.edu.cn

Chunyi Xu
SKLSDE Lab, Beihang University
Beijing, China
zy2106118@buaa.edu.cn

Qianren Mao
Zhongguancun Laboratory
Beijing, China
maoqr@zgclab.edu.cn

Pengpeng Chen
China's Aviation System Engineering
Research Institute
Beijing, China
chenpp@buaa.edu.cn

ABSTRACT

We propose a neuralized undirected graphical model called Neural-Hidden-CRF to solve the weakly-supervised sequence labeling problem. Under the umbrella of probabilistic undirected graph theory, the proposed Neural-Hidden-CRF embedded with a hidden CRF layer models the variables of word sequence, latent ground truth sequence, and weak label sequence with the global perspective that undirected graphical models particularly enjoy. In Neural-Hidden-CRF, we can capitalize on the powerful language model BERT or other deep models to provide rich contextual semantic knowledge to the latent ground truth sequence, and use the hidden CRF layer to capture the internal label dependencies. Neural-Hidden-CRF is conceptually simple and empirically powerful. It obtains new state-of-the-art results on one crowdsourcing benchmark and three weak-supervision benchmarks, including outperforming the recent advanced model CHMM by 2.80 F1 points and 2.23 F1 points in average generalization and inference performance, respectively.

CCS CONCEPTS

• **Mathematics of computing** → *Probabilistic algorithms*; *Markov networks*; • **Computing methodologies** → **Information extraction**; *Natural language processing*.

KEYWORDS

Weak Supervision; Noisy Label; Crowdsourcing; Information Extraction; Sequence Labeling; Named Entity Recognition

*Corresponding author.

1 INTRODUCTION

Deep learning has witnessed the insatiable appetite for humongous labeled training data. This appetite for data motivated several lines of work, such as active learning [23], semi-supervised learning [27], transfer learning [42], and more recently, *weak supervision* (WS) [44, 45], which is of interest in this paper.

As a time/cost-efficient and easy-to-promote alternative to gold expert annotation, WS provides practitioners with *multiple heterogeneous weak supervision sources*, such as crowdsourcing annotators from the Internet, user-defined programs encoded external knowledge bases, patterns/rules, or pre-trained classifiers, etc [28, 44, 45]. As the price of good accessibility and as the name "weak supervision" implies, these various weak sources often exhibit varying error rates, leading to the generation of conflicting and noisy labels in many instances.

WS has been applied to various tasks, including the fundamental deep language understanding task—*sequence labeling* [22], whose importance has been well recognized in the natural language processing community. In this paper, we focus on the problem of sequence learning in the context of multiple heterogeneous weak supervision sources, which can be abbreviated as *weakly-supervised sequence labeling* (WSSL). It has been extensively studied as another main research branch in the whole WS community in addition to normal independent classification tasks [44, 45], because of the importance of the sequence labeling problem itself and the challenges associated with the need to consider the internal dependencies among sequence labels when solving WSSL.

To address the WSSL problem, existing representative methods fall into three categories in intrinsic methodology:

- The HMM-based graphical models [20, 21, 26, 36, 39] leverage the hidden Markov model (HMM) [1] to model the generation process of latent truth label sequence and observed weak label sequence, and then apply the expectation maximization (EM) algorithm [25] to infer truth labels. (Then, these inferred labels, in turn, can be used to train

a final sequence labeler.) Though principled, these models fall short in leveraging token semantics and context information [18], as they either model input tokens as one-hot observations [26, 39] or do not model them at all [20, 21, 36].

- The "source-specific perturbation" deep learning models [17, 26, 46], train multiple weak source-specific deep models, obtained by inserting the *source-specific perturbation parameters* to the *unique shared deep model parameters*, and perform test using the *assumed optimal classifier* obtained by the shared deep model straightforwardly or a certain combination of the source-specific deep models. With less principle, it is not clear how interpretable they are in terms of mechanism design.

- The recently proposed neuralized HMM-based graphical models [18, 19] construct HMM-based directed graphical models in which the dependencies among variables of word sequence, latent ground truth sequences and weak labels are sophisticatedly modeled, and rich contextual semantic information is introduced using deep learning techniques (e.g., the language model BERT [8]).

The neural HMM-based graphical models have the methodological advantages of both the first two classes of approaches—i.e., the principled modeling of graphical models to model variable dependencies and the rich contextual knowledge that comes from using deep learning—and have achieved relatively most satisfactory performance empirically in the recent WS benchmark [45]. However, these methods internally split all the variables of interest into multiple *local* regions and model them separately, and separately model the conditional probabilities of the ground truth at each time step ($p(t_l \mid t_{l-1}, \mathbf{x})$) in the truth sequence. Essentially, this *per-state normalization* approach [16] (coming from the per-step modeling) is the same as that of the MEMM model [24], directly making them suffer from the well-known thorny *label bias problem* [16] that is often mentioned in sequence labeling problems [38, 40, 41]. In short, this approach of using the local optimization perspective (coming from repeatedly considering patterns for the scale of a step instead of holistically considering the entire sequence) causes some useful information to be erased [12] and leads to some bias. In fact, mainly because of this reason, the canonical conditional random field (CRF) [16] was deliberately proposed by scholars in order to solve the sequence labeling problem with a globalized perspective.

In this paper, we move one step further and explore: *when solving the WSSL problem, how can we capitalize on the graphical model with principled modeling of variable dependencies and the advanced deep learning model that can bring rich contextual knowledge, without introducing the label bias problem, in a unified model?* To address this problem, we introduce Neural-Hidden-CRF, a neuralized graphical model embedded with a hidden CRF layer. Neural-Hidden-CRF is built on undirected graph theory and models three sets of variables—namely, word sequence, latent ground truth sequence, and weak label sequence—with a globalized perspective like CRFs instead of the HMM-based models always considering local knowledge. Specifically, in Neural-Hidden-CRF, we use deep learning models (like the language model BERT) to flexibly transfer rich contextual semantic knowledge to the latent truth sequence, and use the embedded hidden CRF layer to capture the dependencies among

the truth sequences, and use the *weak source transition matrices* to model the dependencies between the truth labels and the weak labels. By doing so, our model benefits both from the expressiveness and reasonableness of graphical models for capturing sophisticated dependencies among variables and from the effectiveness of the deep learning models for obtaining contextual semantic knowledge, while avoiding the label bias problem caused by the local perspective. To the best of our knowledge, this is the first work to apply a neuralized undirected graphical model to solve the WSSL problem. We conduct extensive evaluations of the proposed Neural-Hidden-CRF on one crowdsourcing benchmark and three WS benchmarks, showing that Neural-Hidden-CRF is a robust weakly-supervised sequence labeler and outperforms the state-of-the-art. [1]

1.1 Related Work

WSSL Learning Paradigms. To address the WSSL problem, two learning paradigms exist [45]: (1) Two-stage paradigm: Researchers have developed *label models* [20, 21, 26, 36, 39] (also known as *truth inference* models [47]) to aggregate noisy weak labels for each instance, accomplished with an follow-up *end model* (i.e., classifier) learning process using the aggregated labels; (2) Joint paradigm: Later researchers also explored learning the classifier of interest directly from weak supervision labels through ad hoc *joint models* in an end-to-end manner. As presented above, we categorize representative methods from the intrinsic methodological perspective, where each method mentioned in their original work is either emphasized for its truth inference capability [20, 21, 36, 39] or generalization performance [17] or, better yet, both [26, 46].

Other WSSL Works. All WSSL methods can be divided into probabilistic graphical model approach, deep learning model approach, and neuralized graphical model approach. (1) In probabilistic graphical model approach (and in addition to the HMM-based models [20, 21, 26, 36, 39]), Rodrigues et al. [32] in early 2014 used a partially directed graph containing a CRF for modeling to solve the truth inference from crowdsourcing labels; (2) In deep learning model approach (and in addition to the "source-specific perturbation" methods [17, 26, 46]), other methods [17, 33–35] are either based on the end-to-end deep neural architecture [33], or the customized optimization objective along with coordinate ascent optimization technology [34, 35], or the iterative solving framework similar to expectation–maximization algorithm [4]. However, all these methods do not have the advantages of the recently proposed neuralized HMM-based graphical models [18, 19] and our Neural-Hidden-CRF in principled modeling for variants of interest and in harnessing the context information that provided by advanced deep learning models. Additionally, it is worth mentioning the presence of numerous established WS methods that address the normal independent classification scenario [3, 5, 43–45].

2 NEURAL-HIDDEN-CRF

2.1 Problem Formulation and Preliminaries

Problem Formulation of WSSL. We are given i.i.d. training data $\mathcal{D} = \{\mathbf{x}^{(i)}, \mathbf{y}^{(i)}\}_{i=1}^I$, where $\mathbf{x}^{(i)} = \{x_l^{(i)}\}_{l=1}^L \in \mathcal{X}$ is an observed word sequence with L-length tokens, $\mathbf{y}^{(i)} = \{y_l^{(i,j)}\}_{j \in \mathcal{J}^{(i)}, l \in (1,2,\ldots,L)}$

---

[1]The code is available at: https://github.com/junchenzhi/Neural-Hidden-CRF.
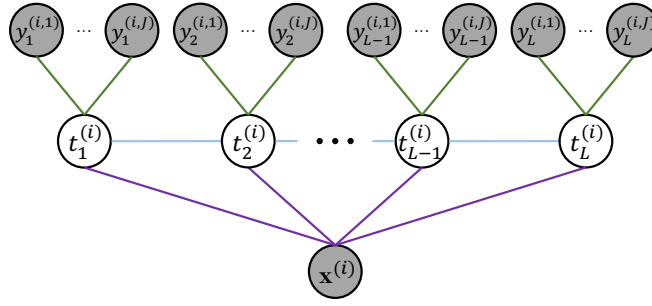
Figure 1: Probabilistic graphical representation of Neural-Hidden-CRF.

are the noisy weak labels attached to i^{th} sentence, and $\mathcal{J}^{(i)}$ represents the set of weak sources that labeled the ith sentence among all J sources. For each sentence $\mathbf{x}^{(i)}$, there is a latent ground truth sequence $\mathbf{t}^{(i)} = \{t_l^{(i)}\}_{l=1}^L \in \mathcal{T}$ *unobserved* to us; $t_l^{(i)} \in \{1, 2, \dots, K\}$, where K denotes number of categories. (In addition, we use $y_l^{(i,j)} = 0$ to denote that source j^{th} has not annotated sentence $\mathbf{x}^{(i)}$.) Our goal is to learn from the weak supervision data $\mathcal{D} = \{\mathbf{x}^{(i)}, \mathbf{y}^{(i)}\}_{i=1}^I$ to obtain a sequence labeler $f : \mathcal{X} \mapsto \mathcal{T}$ with strong generalization.

Preliminaries on Undirected Graphical Models. Here we give the most fundamental overview of the underlying theory (as an optional reading part). **(1)** The set of nodes in an undirected graph, where edges connect any two nodes, is denoted as a *cluster*; if a cluster cannot be added to any node to make it a larger cluster, it is denoted as a *maximum cluster* [15]. **(2)** Under the undirected graphical model theory, the probability distribution over all nodes is factored as the normalized product of *potential functions* of all maximum clusters [15]:

$$p(X) = \frac{1}{Z} \prod_c \phi_c(X_c)$$
$$Z = \sum_X \prod_c \phi_c(X_c), \tag{1}$$

where X_c is the set of nodes in a maximum cluster c, $\phi_c(\cdot)$ is an arbitrary non-negative real-valued function, called the *potential function* (acting as a scoring role), and Z is the normalization factor.

2.2 Model

We first formally introduce our model Neural-Hidden-CRF in Sections 2.2.1- 2.2.3, and briefly explain Neural-Hidden-CRF from another simpler vision in Section 2.2.4. The graphical representation of Neural-Hidden-CRF is shown in Figure 1. Note that in Figure 1 and the presentation (except for the derivation in the Appendix A.1) that follows, we tacitly assume that each instance owns annotations from all weak supervision sources.

2.2.1 Model. In order to present in a more understandable way, we first introduce the base version of the model Neural-Hidden-CRF and then introduce the process of its neuralization in Section 2.2.3 to obtain the eventual neuralized version, i.e., the model we refer to by default. Previously, the CRF [16] was upgraded to its neuralized version (e.g., BiLSTM-CRF [13] or BERT-CRF [45]) by the same neuralization process.

Similar to the original CRF theory [16] and corresponding to Figure 1, we define the probability of weak label sequence $\mathbf{y}^{(i)}$

along with ground truth sequence $\mathbf{t}^{(i)}$ given observation sequence $\mathbf{x}^{(i)}$ to be a normalized product of three kinds of *pseudo-potential function*[2] (which can undergo some simple adaptions to form the strictly potential functions, as mentioned in Seciton 2.1), i.e.,

$$\exp\left(\sum_a \lambda_a \text{state}_a(t_l^{(i)}, \mathbf{x}^{(i)}, l)\right), \tag{2}$$

$$\exp\left(\sum_b \mu_b \text{transition}_b(t_{l-1}^{(i)}, t_l^{(i)}, l)\right), \tag{3}$$

$$\exp\left(\sum_{c,j} \eta_{c,j} \text{source}_{c,j}(y_l^{(i,j)}, t_l^{(i)}, l)\right), \tag{4}$$

where $l \in (1, 2, \dots, L)$ denotes the time step. For now, it is sufficient to note that: **(1)** Within these *pseudo-potential functions*, each of the *feature functions* $\text{state}_a(\cdot)$, $\text{transition}_b(\cdot)$, $\text{source}_{c,j}(\cdot)$—aiming at extracting features—can be the pre-defined indicator function that takes the value 1 when the internal declaration is satisfied, and 0 otherwise; the corresponding *weights* $\lambda_a, \mu_b, \eta_{c,j} \in (-\infty, +\infty)$ are model's parameters to be estimated; **(2)** These exponential *pseudo-potential functions* play the role of scoring (for a specific instantiated value of $\mathbf{x}^{(i)}, \mathbf{t}^{(i)}, \mathbf{y}^{(i)}$ on every time step) and will be non-negative. In other words, the internal *feature functions* along with their weights play the role of scoring; **(3)** Intuitively, the three types of *feature functions*, $\text{state}_a(\cdot)$, $\text{transition}_b(\cdot)$, $\text{source}_{c,j}(\cdot)$—corresponding to purple lines, blue lines, and green lines in Figure 1—act between the token sequence $\mathbf{x}^{(i)}$ and the truth $\mathbf{t}^{(i)}$, between the interior of the truth sequence $\mathbf{t}^{(i)}$, and between the truth $\mathbf{t}^{(i)}$ and the weak labels $\mathbf{y}^{(i)}$, respectively. Specifically, we will walk through more details about *features functions* in Section 2.2.2.

For simplicity, we denote the above three *feature functions* and the corresponding *weights* by the general notations:

$$f_w(\mathbf{y}_l^{(i)}, t_{l-1}^{(i)}, t_l^{(i)}, \mathbf{x}^{(i)}, l) =$$

$$\begin{cases} \text{state}_a(t_l^{(i)}, \mathbf{x}^{(i)}, l) & \text{if } w = 1, .., A \\ \text{transition}_b(t_{l-1}^{(i)}, t_l^{(i)}, l) & \text{if } w = A+1, .., A+B \\ \text{source}_{c,j}(y_l^{(i,j)}, t_l^{(i)}, l) & \text{if } w = A+B+1, .., A+B+\sum_j C_j, \end{cases}$$
$$\tag{5}$$

---

[2]Note that for the sake of clarity, here we do not start with the construction of our *potential functions* in the strict sense, as mentioned in Section 2.1. Instead, we create and define the "pseudo-potential function", which is similar to the strict *potential function*, but its role is not equivalent to that of a strictly defined one.

along with

$$\theta_w = \begin{cases} \lambda_a & \text{if } w = 1, .., A \\ \mu_b & \text{if } w = A + 1, ..., A + B \\ \eta_{c,j} & \text{if } w = A + B + 1, ..., A + B + \sum_j C_j, \end{cases} \quad (6)$$

where A, B, and $\sum_j C_j$ denote the specific number of a certain type of feature function, respectively.

Thus, our conditional model can be expressed as:

$$p(\mathbf{y}^{(i)}, \mathbf{t}^{(i)} \mid \mathbf{x}^{(i)}; \Theta)$$

$$= \frac{1}{Z(\mathbf{x}^{(i)}; \Theta)} \exp\left(\sum_l \sum_w \theta_w \cdot f_w(\mathbf{y}_l^{(i)}, t_{l-1}^{(i)}, t_l^{(i)}, \mathbf{x}^{(i)}, l)\right), \quad (7)$$

where $Z(\mathbf{x}^{(i)}; \Theta)$ is the instance-specific normalization factor (also called *partition function* in the CRF [16]) defined as:

$$Z(\mathbf{x}^{(i)}; \Theta) = \sum_{\mathbf{y}^{(i)}} \sum_{\mathbf{t}^{(i)}} \exp\left(\sum_l \sum_w \theta_w \cdot f_w(\mathbf{y}_l^{(i)}, t_{l-1}^{(i)}, t_l^{(i)}, \mathbf{x}^{(i)}, l)\right). \quad (8)$$

More intuitively, if $\exp\left(\sum_l \sum_w \theta_w \cdot f_w(\mathbf{y}_l^{(i)}, t_{l-1}^{(i)}, t_l^{(i)}, \mathbf{x}^{(i)}, l)\right)$, representing getting the score for a specific instantiation of $(\mathbf{y}^{(i)}, \mathbf{t}^{(i)}, \mathbf{x}^{(i)})$, abbreviated with $\Phi(\mathbf{y}^{(i)}, \mathbf{t}^{(i)}, \mathbf{x}^{(i)})$, then Equation 7 can be rewritten as:

$$p(\mathbf{y}^{(i)}, \mathbf{t}^{(i)} \mid \mathbf{x}^{(i)}; \Theta) = \frac{\Phi(\mathbf{y}^{(i)}, \mathbf{t}^{(i)}, \mathbf{x}^{(i)})}{\sum_{\mathbf{y}^{(i)}} \sum_{\mathbf{t}^{(i)}} \Phi\left(\mathbf{y}^{(i)}, \mathbf{t}^{(i)}, \mathbf{x}^{(i)}\right)}. \quad (9)$$

Essentially, our model given by Equation 7 or Equation 9 is inherently aligns with the underlying theory mentioned in Section 2.1.[3]

The Embodiment of the Global Optimization Perspective. We can notice that the our pseudo-potential functions and feature functions in Equations 2-3 do not have a direct probabilistic interpretation, but instead represent constraints or scores on the configurations of the random variable. As a result, the model expressed by Equation 7 yields a *global normalized score* for $p(\mathbf{y}^{(i)}, \mathbf{t}^{(i)} \mid \mathbf{x}^{(i)}; \Theta)$. This *global normalization* approach is unlike all HMMs, where $(\mathbf{y}^{(i)}, \mathbf{t}^{(i)})$ is split into multiple uni-directional dependent random variables (i.e., a set consisting of many $(y_l^{(i,j)}, t_l^{(i)})$) based on some strict independence assumptions and each conditional probability distribution between random variables is normalized (e.g., *local normalization* for per-step in Li et al. [18, 19]) to further obtain the probability of the joint distribution $(\mathbf{y}^{(i)}, \mathbf{t}^{(i)})$. Simply put, our approach models/trains holistically (the learned knowledge is global), while the HMMs [18, 19] decompose the modeling into multiple uni-directional dependent local regions and model the patterns for the scale of a step (the learned knowledge is local). As a result of the holistic undirected graphical modeling, our method can result in model parameters that are not constrained by probabilistic forms, thus enjoying more flexible scoring. As for the *label bias problem*, our model circumvents this by adopting the *global normalization* rather than the *local normalization* in Li et al. [18, 19], just as the CRF model does with respect to the MEMM model [12, 16]. Please refer to Hannun [12] for more information on the label bias problem.

---

[3] Referring to more material on CRFs and our tutorial (https://github.com/junchenzhi/Neural-Hidden-CRF) would help to enhance the comprehension of our model.

2.2.2 Feature Functions.
(1) For feature function $\text{state}_a(\cdot)$, like the original CRF theory, we can define the following example:

$$\text{state}_a(t_l^{(i)}, \mathbf{x}^{(i)}, l) = \begin{cases} 1 & \text{if } t_l^{(i)} = \text{PERSON and } x_l^{(i)} = \text{John} \\ 0 & \text{otherwise.} \end{cases} \quad (10)$$

If the corresponding weight λ_a is a relatively large value, whenever the internal declaration in $\text{state}_a(\cdot)$ is true, it increases the probability of the sequence $\mathbf{t}^{(i)}$. Intuitively, the model would prefer the tag PERSON for the word John. Formally, whenever the internal declaration in $\text{state}_a(\cdot)$ is satisfied, this feature function along with its weights λ_a will contribute factor $\exp(\lambda_a \cdot 1)$ to the numerator in Equation 7.

(2) For feature function $\text{transition}_b(\cdot)$, we can define the following example:

$$\text{transition}_b(t_{l-1}^{(i)}, t_l^{(i)}, l) = \begin{cases} 1 & \text{if } t_{l-1}^{(i)} = \text{OTHER and } t_l^{(i)} = \text{PERSON} \\ 0 & \text{otherwise.} \end{cases} \quad (11)$$

Also, whenever the internal declaration in $\text{transition}_b(\cdot)$ is satisfied, this feature function along with its weights μ_b will contribute factor $\exp(\mu_b \cdot 1)$ to the numerator in Equation 7. Since the number of categories is K, naturally we can define all K^2 feature functions of $\text{transition}_b(\cdot)$. The set of parameters concerning $\text{transition}_b(\cdot)$ can referred to as the *CRF transition matrix* (with size of $K \times K$), which essentially captures the dependence within the label sequence.

(3) For feature function $\text{source}_{c,j}(\cdot)$, we can define the following example:

$$\text{source}_{c,j}(y_l^{(i,j)}, t_l^{(i)}, l) = \begin{cases} 1 & \text{if } y_l^{(i,j)} = \text{PERSON and } t_l^{(i)} = \text{PERSON} \\ 0 & \text{otherwise.} \end{cases} \quad (12)$$

Similar to feature function $\text{transition}_b(\cdot)$, we can define all K^2 feature functions of $\text{source}_{c,j}(\cdot)$ for weak source j^{th}. For the particular j^{th} source, weights $\{\eta_{c,j}\}_{c=1}^{K^2}$ naturally form a $K \times K$ matrix that can represents the behavior pattern of this source. Thus, the higher the ability of a source, the larger the value of the diagonal elements of its matrix relative to the value of the non-diagonal elements. Similar to the *CRF transition matrix*, we can refer to this matrix as *weak source transition matrix*.

2.2.3 Eventually Neuralized Model.
Here we introduce a deep sequence network, such as the language model BERT without the last softmax layer, between sequence $\mathbf{x}$ and sequence $\mathbf{t}$ to complete the model's neuralization. Thus: (*i*) In the basic version of the model described above, for the time step l in the sentence $\mathbf{x}^{(i)}$, the feature function $\text{state}_a(\cdot)$ along with it's weight λ_a provide the factor $\exp(\lambda_a \cdot \text{state}_a(t_l^{(i)}, \mathbf{x}^{(i)}, l))$—which represents the degree of support of the model for $(\mathbf{x}_l^{(i)}, t_l^{(i)})$—for the numerator in Equation 7; (*ii*) In the current neuralized model, we use

$$\text{extract}_{l, t_l^{(i)}}(\sigma_{BERT}(\mathbf{x}^{(i)})), \quad (13)$$

which also represents the degree of support of the model for $(\mathbf{x}_l^{(i)}, t_l^{(i)})$, as the factor provided to the numerator in Equation 7. In Equation 13, $\sigma_{BERT}(\cdot)$ is the output logits of BERT, and $\text{extract}_{l, t_l^{(i)}}(\cdot)$ extracts the probability mass of the category $t_l^{(i)}$ in the l-step element of the input.

2.2.4 Understanding Our Model from a Simpler Perspective. Our
Neural-Hidden-CRF, for weakly-supervised sequence labeling learn-
ing, shares similarities with CRFs (e.g., BERT-CRF), for supervised
sequence labeling learning. We show the graphical representation
of CRF vs. Neural-Hidden-CRF in Appendix A.2. **(1)** First, BERT-
CRF is a discriminative model concerning the label sequence $\mathbf{t}^{(i)}$
given the sentence $\mathbf{x}^{(i)}$:

$$p(\mathbf{t}^{(i)} \mid \mathbf{x}^{(i)}; \Theta) = \frac{\exp(\text{score}_\Theta(\mathbf{t}^{(i)}, \mathbf{x}^{(i)}))}{\sum_{\mathbf{t}^{(i)}} \exp(\text{score}_\Theta(\mathbf{t}^{(i)}, \mathbf{x}^{(i)}))}, \quad (14)$$

$$\text{score}_\Theta(\mathbf{t}^{(i)}, \mathbf{x}^{(i)}) = \sum_{l=1}^{L} (\text{Emission}_{l, t_l^{(i)}} + \text{CrfTransition}_{t_{l-1}^{(i)}, t_l^{(i)}}), \quad (15)$$

where $\text{Emission} \in \mathbb{R}^{L \times K}$ is the *emission score matrix* coming from
the logit outputs of BERT ($\text{Emission} = f_{\Theta_{\mathbf{BERT}}}(\mathbf{x}^{(i)})$), and CrfTran-
sition $\in \mathbb{R}^{K \times K}$ is the *CRF transition matrix*. Model parameters are
$\Theta = \{\Theta_{\mathbf{BERT}}, \text{CrfTransition}\}$. **(2)** Similarly, our proposed Neural-
Hidden-CRF is also a exponential discriminative model, concerning
the weak label sequence $\mathbf{y}^{(i)}$ and label sequence $\mathbf{t}^{(i)}$ given the
sentence $\mathbf{x}^{(i)}$:

$$p(\mathbf{y}^{(i)}, \mathbf{t}^{(i)} \mid \mathbf{x}^{(i)}; \Theta) = \frac{\exp(\text{score}_\Theta(\mathbf{y}^{(i)}, \mathbf{t}^{(i)}, \mathbf{x}^{(i)}))}{\sum_{\mathbf{y}^{(i)}} \sum_{\mathbf{t}^{(i)}} \exp(\text{score}_\Theta(\mathbf{y}^{(i)}, \mathbf{t}^{(i)}, \mathbf{x}^{(i)}))}, \quad (16)$$

$$\text{score}_\Theta(\mathbf{y}^{(i)}, \mathbf{t}^{(i)}, \mathbf{x}^{(i)}) = \sum_{l=1}^{L} (\text{Emission}_{l, t_l^{(i)}} + \text{CrfTransition}_{t_{l-1}^{(i)}, t_l^{(i)}} +$$

$$\text{WeakSourceTransition\#1}_{t_l^{(i)}, y_l^{(i,1)}} + ... + \text{WeakSourceTransition\#J}_{t_l^{(i)}, y_l^{(i,J)}}), \quad (17)$$

where Emission, CrfTransition have the same meaning as those
in model BERT-CRF above, and each WeakSourceTransition $\in$
$\mathbb{R}^{K \times K}$ refers to the *weak source transition matrix* introduced in
Section 2.2.2. Model parameters are $\Theta = \{\Theta_{\mathbf{BERT}}, \text{CrfTransition},$
$\text{WeakSourceTransition\#1}, ..., \text{WeakSourceTransition\#J}\}$.

2.3 Learning

Given the weak supervision data $\mathcal{D} = \{\mathbf{x}^{(i)}, \mathbf{y}^{(i)}\}_{i=1}^{I}$ and the model
constructed above, we estimate the parameters of the model by max-
imizing the conditional log-likelihood involving the latent ground
truth variable:

$$\mathcal{L}(\Theta) = \sum_i \log p(\mathbf{y}^{(i)} \mid \mathbf{x}^{(i)}; \Theta). \quad (18)$$

Further,

$$\log p(\mathbf{y}^{(i)} \mid \mathbf{x}^{(i)}; \Theta)$$
$$= \log \sum_{\mathbf{t}^{(i)}} p(\mathbf{y}^{(i)}, \mathbf{t}^{(i)} \mid \mathbf{x}^{(i)}; \Theta)$$
$$= \log \frac{1}{Z(\mathbf{x}^{(i)}; \Theta)} \sum_{\mathbf{t}^{(i)}} \exp \left(\sum_l \sum_w \theta_w \cdot f_w(\mathbf{y}_l^{(i)}, t_{l-1}^{(i)}, t_l^{(i)}, \mathbf{x}^{(i)}, l) \right), \quad (19)$$

where instance-specific normalization factor $Z(\mathbf{x}^{(i)}; \Theta)$ defined
before is

$$Z(\mathbf{x}^{(i)}; \Theta) = \sum_{\mathbf{y}^{(i)}} \sum_{\mathbf{t}^{(i)}} \exp \left(\sum_l \sum_w \theta_w \cdot f_w(\mathbf{y}_l^{(i)}, t_{l-1}^{(i)}, t_l^{(i)}, \mathbf{x}^{(i)}, l) \right). \quad (20)$$

Calculation of $\log \sum_{\mathbf{t}^{(i)}} \exp \left(\sum_l \sum_w \theta_w \cdot f_w(\mathbf{y}_l^{(i)}, t_{l-1}^{(i)}, t_l^{(i)}, \mathbf{x}^{(i)}, l) \right)$
and $\log Z(\mathbf{x}^{(i)}; \Theta)$—similar to the corresponding calculation of the
CRF—can be efficiently solved by dynamic programming algorithm.
The detail derivations are shown in Appendix A.1.

The above $\mathcal{L}(\Theta)$ provides a unified objective function for opti-
mization in Neural-Hidden-CRF, which can be done with standard
stochastic optimization techniques, such as SGD [11] or Adam [14].

2.4 Inference

At the test phase, given a new test sequence $\mathbf{x}$, we want to infer the
most probable ground truth sequence $\mathbf{t}^* = \arg\max_{\mathbf{t}^*} p(\mathbf{t}^* \mid \mathbf{x}; \Theta)$.
Here we can ignore the parameters of the weak source transition
matrix part and use the classifier (e.g., BERT-CRF or BiLSTM-CRF)
within Neural-Hidden-CRF to make the inference. Like the CRFs,
this inference problem can be solved efficiently with the canonical
Viterbi algorithm [9], which applies the dynamic programming.

2.5 Implementation Details

Parameter initialization. In our model, similar to the initialization
in weak supervision model MAX-MIG [2], we can initialize the
parameters of the weak sources (i.e., the *weak source transition
matrix*, denoted as $\Pi^{(j)}$) as:

$$\pi_{mn}^{(j)} = \rho \cdot \frac{\sum_{i=1}^{I} \sum_{l=1}^{L} \mathbb{I}(t_l^{(i)} = m) \mathbb{I}(y_l^{(i,j)} = n)}{\sum_{i=1}^{I} \sum_{l=1}^{L} \mathbb{I}(t_l^{(i)} = m) \mathbb{I}(y_l^{(i,j)} \neq 0)}, \quad (21)$$

where ρ is a hyper-parameter and $t_l^{(i)}$ can be easily obtained by
majority voting method. In addition, for the parameters of the
classifier part (i.e., parameters in Neural-Hidden-CRF other than
the weak source transition matrices), we can easily pre-train the
classifier using the labels inferred by majority voting to obtain a
better parameter initialization for the model.

2.6 Others: Computational Complexity

The computational complexities of our method and some repre-
sentative methods are shown in Table 1, which contains the com-
plexities of (1) performing the probability calculation on likeli-
hood/objective during learning and (2) performing inference. In
summary, our method has the same complexities as many existing
methods.

Table 1: Computational Complexity. $L/K/J$: **sequence length/#
categories/# weak sources.**

Method	Probability calculation	Inference
MV + BERT-CRF[§]	$O(LK^2)$	$O(LK^2)$
LSTM-Crowd [26][*], LSTM-Crowd-cat [26][*] CONNET [17][*], Zhang et al. [46][*]	$O(JLK^2)$	$O(LK^2)$
Ours[*]	$O(JLK^2)$	$O(LK^2)$

[1] §: When we use the labels inferred from a truth inference method and perform supervised training, e.g.,
MV+BERT-CRF, the complexities of MV+BERT-CRF are the same as CRF [6].

[2] *: Our method has the same complexities as the "source-specific perturbation" methods LSTM-Crowd [26],
LSTM-Crowd-cat [26], CONNET [17] and Zhang et al. [46]. This is because: (*i*) For the probability
calculation complexity, since the "source-specific perturbation" methods require to learn J source-specific
models, their complexities ($O(JLK^2)$) are J times the corresponding complexity of CRF ($O(LK^2)$). Also,
when our method utilizes the dynamic programming algorithm to compute our Equation A.3 (the most
significant consumers of computing) in the Appendix A.1, its complexity is also $O(JLK^2)$; (*ii*) For the
inference complexity, each Viterbi decoding process required by these methods is the same as for the
CRF, and therefore the complexities are all $O(LK^2)$.

[3] Note that here we consider the complexities on one instance, and by the general convention, we do not
consider the complexity arising from the deep neural backbone, which has an equivalent effect for all
methods.

3 EXPERIMENTS

3.1 Setup

3.1.1 Datasets. We evaluate the proposed Neural-Hidden-CRF on four widely-used, publicly available WS datasets, including the CoNLL-03 (MTurk) dataset [32, 33] contributed by crowdsourcing workers from Amazon Mechanical Turk (MTurk)[4], and three datasets [45] (CoNLL-03 (WS), WikiGold (WS), MIT-Restaurant (WS)) labeled from artificially pre-defined label functions. Table 2 shows the main statistics. Specifically: **(1) CoNLL-03 (MTurk)** [32, 33] is constructed on the well-established CoNLL-03 dataset [37] through introducing additional crowdsourcing annotations. The goal is to recognize named entities (*person, location, organization, miscellaneous*) together with their different parts (*begin, inside*) in the sentence. We shuffled and divided the original 3250 test samples in Rodrigues et al. [32] into a validation set and a test set containing 2000/1250 samples, respectively; **(2) CoNLL-03 (WS), WikiGold (WS) and MIT-Restaurant (WS)** are utilized and open-sourced in the recently proposed WS benchmark called Wrench [33, 45]. These three datasets cover three different domains, and detailed information about them is provided in Zhang et al. [45].

Table 2: Statistics of all datasets.

Dataset	Domain	#Data(train/val/test)	#Entities	#Source
CoNLL (MTurk)	News	5,985/2,000/1,250	4	47
CoNLL (WS)	News	14,041/3,250/3,453	4	16
WikiGold (WS)	Web Text	1,355/169/170	4	16
MIT-Rest. (WS)	Review	7,159/500/1,521	8	16

3.1.2 Compared Methods. **(1) On CoNLL-03 (MTurk).** We consider the following methods: (*i*) MV-BiLSTM/MV-BiLSTM-CRF: They are the two-stage learning baselines, which first estimate the ground truth from weak labels by MV (Majority Voting), and then train the LSTM/LSTM-CRF; (*ii*) CL (VW), CL (VW+B) and CL (MW): They are three variants of the representative WSSL method Crowd-Layer [33], where "VW", "VW+B" and "MW" refer to three different ways of parameterizing weak source reliability; (*iii*) LSTM-Crowd [26], LSTM-Crowd-cat [26], Zhang et al. [46], and CONNET [17]: These four methods, which apply the "source-specific perturbation" mentioned in Section 1, dominate the deep learning-based WSSL methods and show the competitive results [17]; (*iv*) OptSLA [34] and AggSLC [35]: They both follow the approach of constructing an optimization objective containing weak source weights, classifier parameters, latent ground truth, and iteratively updating them using a coordinate ascent algorithm; (*v*) CRF-MA [31]: This is a partial directed graphical model where the ground truth sequence is also modeled as a latent variable and each weak source's behavior pattern is modeled by a specific scalar; (*vi*) HMM-Crowd [26] and BSC-seq [39]: They belong to the HMM-based graphical models mentioned in Section 1, where the latter is a Bayesian version of the former; (*vii*) Finally, we consider Gold, denoting the classifier (BiLSTM-CRF) trained in the ideal case when true labels are known. **(2) On CoNLL-03 (WS), WikiGold (WS) and MIT-Restaurant (WS).** We compared many methods by using

the results reported from benchmark Wrench [45]. Specifically, they involves the advanced CONNET [17], CHMM [18], the HMM-based graphical model called HMM [21], and the label models (WMV [45], DS [7], DP [30], MeTal [29], FS [10]) for classification task with certain adaptations.

3.1.3 Configurations. The hyper-parameter settings are shown in Appendix A.3. (Also, note that some suggestions for setting hyper-parameters are provided in Appendix A.4.) Further: **(1) On CoNLL-03 (MTurk).** We applied the canonical BiLSTM-CRF [22][5] as the classifier backbone of our model and comparison methods. **(2) On CoNLL-03 (WS), WikiGold (WS) and MIT-Restaurant (WS).** Our experiments on these datasets build on the recent great benchmark Wrench [45], where we adhered rigorously to their various settings and used their open-source code as the foundation for implementing our method. We used the more advanced language model BERT of the two available choices (BiLSTM and BERT) provided by Wrench as the backbone.

3.2 Results and Analysis

3.2.1 Main Results. Tables 3 and 4—concerning the CoNLL-03 (MTurk) dataset and the other three WS datasets, respectively—show the prediction performance of all methods on the test data and the inference performance on the training/test data, i.e., the performance of inferring the latent ground truth.[6] First, *we find that our model Neural-Hidden-CRF substantially outperforms all the comparison methods by a large margin on the most important average F1 metric on dataset CoNLL-03 (MTurk) and the other three datasets.* The more robust performance demonstrated by our Neural-Hidden-CRF relative to the SOTA neuralized HMM-based CHMM [18] largely showcases the effectiveness of our model in leveraging the global optimization perspective offered by the undirected graphical model. Further and more specifically, on the average F1 metric, Neural-Hidden-CRF outperforms the recently proposed AggSLC [35] by 4.81 points on CoNLL-03 (MTurk), and exceeds the SOTA method CHMM [18] by 2.80/2.23 points on the three WS datasets. It is also worth noting that the comparison methods [17, 26, 35, 46] on CoNLL-03 (MTurk) dataset, apply either the same backbone (i.e., the GloVe 100-dimensional word embeddings along with BiLSMT-CRF in Nguyen et al. [26]) as ours, or more advanced backbones (i.e., BERT-BiLSTM-CRF in Zhang et al. [46], Efficient ELMO along with BiLSTM-CRF in Lan et al. [17], BERT in AggSLC [35]) than ours.

Compared with the inference metrics, we are more interested in prediction metrics, because in general, our ultimate objective revolves around developing a robust sequence labeler endowed with strong generalization. For the prediction metric, we find that our Neural-Hidden-CRF outperforms all comparison methods across all datasets, often with considerable margins. In terms of inference performance, in addition to achieving the second-best result on the MIT-Restaurant (WS) dataset, Neural-Hidden-CRF still often maintains a significant lead on the remaining three datasets and outperforms the second-best by 1.49/4.77/0.80 points.

---

[4]https://www.mturk.com/

[5]We used the publicly available implementation: https://github.com/ZubinGou/NER-BiLSTM-CRF-PyTorch.

[6]It is worth noting that, unlike the metrics of "inference on train data" in Table 3 and consistent with the approach in the WS benchmark [45], we report in Table 4 the inference performance of all methods on the test data, where weak labels are also available.

Table 3: Performance (%) on CoNLL-03 (MTurk) dataset. Results are averaged over 20 runs. The best results under the F1 metric of most interest are marked in bold.

Paradigm	Method	Prediction on test data§			Inference on train data*			Avg. F1
		Precision	Recall	F1	Precision	Recall	F1	
Two-stage WSSL	MV + BiLSTM-CRF	87.19(±1.19)	65.00(±3.28)	74.41(±2.11)	86.27(±1.08)	66.06(±2.3)	74.79(±1.38)	74.60
	MV + BiLSTM	82.21(±1.46)	61.30(±2.57)	70.20(±1.69)	80.62(±1.01)	61.82(±2.36)	69.96(±1.64)	70.08
One-stage WSSL	CL (VW) [33]	83.93(±0.83)	61.50(±2.07)	70.96(±1.46)	82.90(±0.71)	64.02(±1.76)	72.24(±1.29)	71.60
	CL (VW+B) [33]	81.93(±1.57)	61.00(±2.89)	69.87(±1.62)	80.31(±1.38)	61.70(±2.65)	69.75(±1.73)	69.81
	CL (MW) [33]	83.93(±0.89)	61.33(±1.65)	70.86(±1.65)	82.24(±0.55)	62.91(±1.26)	71.27(±0.88)	71.07
	LSTM-Crowd [26]†	82.38	62.10	70.82	-	-	-	-
	LSTM-Crowd-cat [26]†	79.61	62.87	70.26	-	-	-	-
	Zhang et al. [46]†	78.84	75.67	77.95	-	-	-	-
	CONNET [17]†	87.77(±0.25)	72.79(±0.04)	79.99(±0.08)	-	-	-	-
	AggSLC [35]†	70.95	77.16	73.93	83.02	78.69	80.79	77.36
	CRF-MA [32]†	49.4	85.6	62.6	86.0	65.6	74.4	68.5
	Neural-Hidden-CRF	82.25(±1.05)	80.93(±1.05)	**82.06**(±0.63)	84.41(±1.04)	80.28(±0.74)	**82.28**(±0.49)	**82.17**
Truth Inference	MV	-	-	-	79.12(±0.00)	58.50(±0.00)	67.27(±0.00)	-
	OptSLA [34]†	-	-	-	79.42	77.59	78.49	-
	HMM-Crowd [26]†	-	-	-	77.40	72.29	74.76	-
	BSC-seq [39]†	-	-	-	80.3	74.8	77.4	-
-	Gold (Upper Bound)	91.94(±0.66)	91.49(±0.87)	91.71(±0.75)	100	100	100	95.86

[1] §/*: Learn from weak supervision labels on the train data and predict on the test data/learn from weak supervision labels on the train data and infer the latent ground truth labels.
[2] †: Results are reported from the original works. Note that there are some blanks in these results, as most of these methods reported one of two metrics in their original works.

Table 4: Performance (%) on WS benchmark datasets from Zhang et al. [45]. Our results are averaged over 20 runs. The best results are marked in bold. Each table cell contains F1 score with standard deviation and (Precision, Recall) in the bracket.

Paradigm	Method	Prediction on test data§			Inference on test data*			Avg.F1(P/I)
		CoNLL-03	WikiGold	MIT-Rest.	CoNLL-03	WikiGold	MIT-Rest.	
Two-stage WSSL	MV + BERT-CRF [45]†	66.63(±0.85) (67.68/65.62)	62.09(±1.06) (61.89/62.29)	42.95(±0.43) (63.18/32.54)	60.36(±0.00) (59.06/61.72)	52.24(±0.00) (48.95/56.00)	**48.71**(±0.00) (74.25/36.24)	57.22/53.77 -
	WMV + BERT-CRF [45]†	64.38(±1.09) (66.55/62.35)	59.96(±1.08) (60.33/59.73)	42.62(±0.23) (63.56/32.06)	60.26(±0.00) (59.03/61.54)	52.87(±0.00) (50.74/55.20)	48.19(±0.00) (73.73/35.80)	55.65/53.77 -
	DS + BERT-CRF [7]†	53.89(±1.42) (54.10/53.68)	48.89(±1.59) (46.80/51.20)	42.26(±0.78) (62.65/31.89)	46.76(±0.00) (45.29/48.32)	42.17(±0.00) (40.05/44.53)	46.81(±0.00) (71.71/34.75)	48.35/42.25 -
	DP + BERT-CRF [30]†	65.48(±0.37) (66.76/64.28)	61.09(±1.53) (61.07/61.12)	42.27(±0.53) (62.81/31.86)	62.43(±0.22) (61.62/63.26)	54.81(±0.13) (53.10/56.64)	47.92(±0.00) (73.24/35.61)	56.28/55.05 -
	MeTal + BERT-CRF [29]†	65.11(±0.69) (66.87/63.45)	58.94(±3.22) (61.53/56.75)	42.26(±0.49) (62.82/31.84)	60.32(±0.08) (59.07/61.63)	52.09(±0.23) (50.31/54.03)	47.66(±0.00) (73.40/35.29)	55.44/53.37 -
	FS + BERT-CRF [10]†	67.34(±0.75) (70.05/64.83)	66.44(±1.40) (72.86/61.17)	13.80(±0.23) (72.63/7.62)	62.49(±0.00) (63.25/61.76)	58.29(±0.00) (62.77/54.40)	13.86(±0.00) (84.20/7.55)	49.19/44.88 -
	HMM + BERT-CRF [21]†	67.49(±0.89) (71.26/64.14)	63.31(±1.02) (70.95/57.33)	39.51(±0.72) (62.49/28.90)	62.18(±0.00) (66.42/58.45)	56.36(±0.00) (61.51/52.00)	42.65(±0.00) (71.44/30.40)	56.77/53.73 -
	CHMM + BERT-CRF [18]†	66.72(±0.41) (67.17/66.27)	63.06(±1.91) (62.12/64.11)	42.79(±0.22) (63.19/32.35)	63.22(±0.26) (61.93/64.56)	58.89(±0.97) (55.71/62.45)	47.34(±0.57) (73.05/35.02)	57.52/56.48 -
One-stage WSSL	CONNET [17]†	67.83(±0.62) (69.37/66.40)	64.18(±1.71) (72.17/57.92)	42.37(±0.72) (62.88/31.95)	- -	- -	- -	58.13/- -
	Neural-Hidden-CRF	**69.16**(±0.92) (73.13/65.64)	**66.87**(±1.79) (73.00/61.87)	**44.94**(±0.99) (58.27/36.66)	**67.99**(±0.58) (73.12/63.55)	**59.69**(±0.68) (71.23/51.44)	48.44(±0.86) (68.17/37.85)	**60.32/58.71** -
-	Gold + BERT-CRF†	87.38(±0.34) (87.70/87.06)	86.78(±0.84) (87.27/86.29)	78.83(±0.44) (79.14/78.53)	100.00(±0.00) (100.00/100.00)	100.00(±0.00) (100.00/100.00)	100.00(±0.00) (100.00/100.00)	84.33/100.00 -

[1] §/*: Learn from weak supervision labels on the train data and predict on the test data/directly learn from weak supervision labels available on the test data and infer the ground truth labels.
[2] †: Results are reported from Zhang et al. [45].
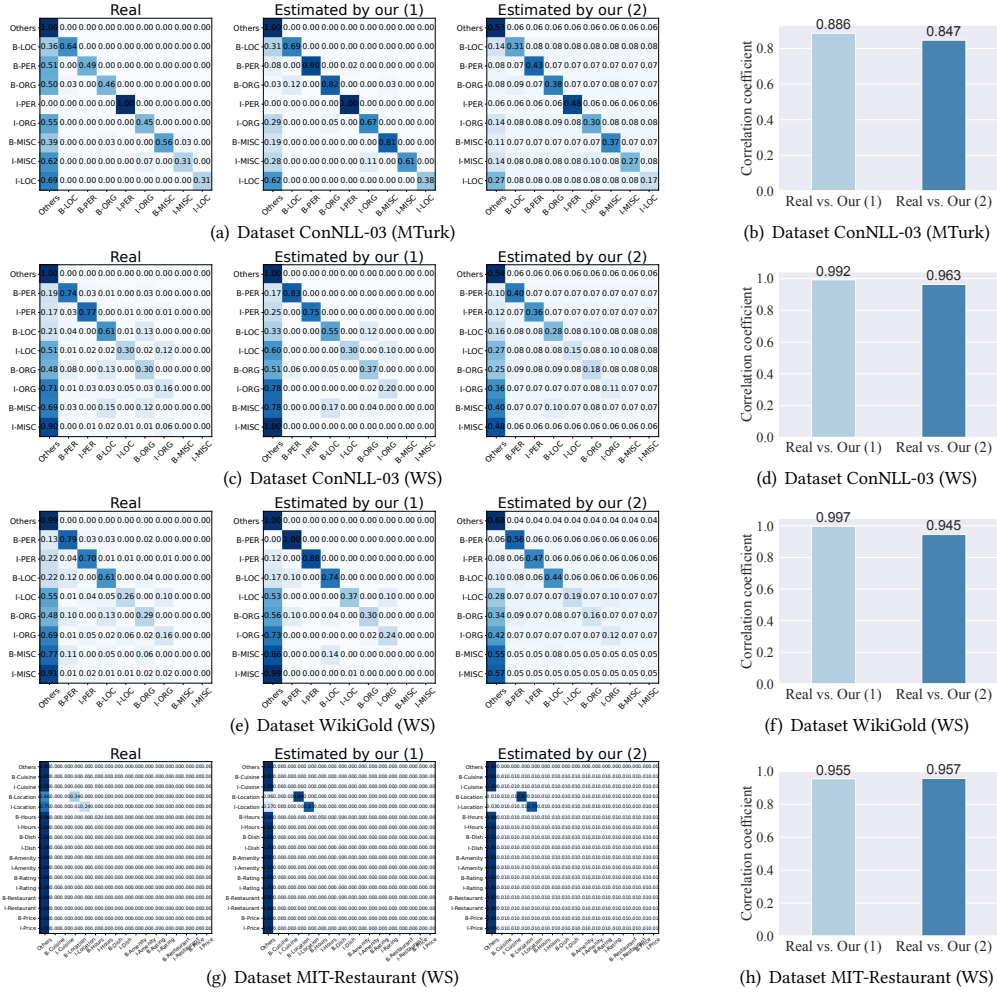
Figure 2: Comparison between the real weak source transition matrix and the two weak source transition matrices estimated by Neural-Hidden-CRF on the four datasets. (*i*) Real: it denotes the probabilistic confusion matrix that we compute by using the truth labels and weak labels in the dataset (in fact, we cannot obtain the real matrix under the theory of our model); (*ii*) Our (1): it is obtained by setting all non-positive elements of the weak source transition matrix to 0 and normalizing the elements on each row; (*iii*) Our (2): it is obtained by exponentiating all elements of the weak source transition matrix and normalizing the elements on each row; (*iv*) In each sub-figure on correlation coefficient, we calculate the element-level values.

3.2.2 Weak Source Parameter Estimation and Interpretability.

Benefiting from our use of the interpretable weak source transition matrices in the neuralized undirected graphical model rather than hard-to-interpret neural network parameters to model weak source behavior patterns, we can now conduct a post-hoc study for the estimated matrices. Methodologically, for each specific weak supervision source, its parameters can form a matrix of size $K \times K$. These parameters possess interpretability on the behavioral pattern of the source. That is, the matrix's element at position (i, j) denotes scoring information for the case when the truth is i and the weak label is j, where a larger value reflects a greater likelihood. Empirically, Figure 2 shows the results for the respective first weak source on the four datasets. These results substantiate the accuracy of estimating the weak source transition matrices, and validate that the weak

source transition matrices we model do have the *interpretability* in expressing the label transition patterns of weak sources (similar to the CRF transition matrix in the CRF model [16]). Also, such a result further demonstrates the effectiveness of Neural-Hidden-CRF from another side. In additin, the parameters of the weak source transition matrices estimated in Figure 2 are unrestricted (i.e., each parameter takes the value space of $(-\infty, +\infty)$), without satisfying probabilistic statutes (as in the HMMs). Also, our CRF transition matrix is similar. For example, the elements in the first row of our estimated CRF transition matrix on CoNLL-03 (MTurk) are $[0.24, 2.94, 2.57, 1.69, -3.18, -4.29, 1.11, -3.57, -3.09]$. These illustrate the resulting flexible scoring comes from the mechanism of holistic undirected graphical modeling and holistic parameter configuration.

Table 5: Performance (F1, %) on ablation study. Results are averaged over 10 runs.

Method	CoNLL-03(MTurk) (P/I)§	CoNLL-03(WS) (P/I/I)*	WikiGold(WS) (P/I/I)*	MIT-Restaurant(WS) (P/I/I)*	Avg.(P/I/I)*
W/o-weak-transition	74.41(±2.11)/74.79(±1.38)	66.63(±0.85)/68.61(±0.72)/65.43(±0.51)	62.09(±1.06)/60.82(±1.76)/52.32(±0.26)	42.95(±0.43)/45.00(±0.71)/48.01(±0.73)	61.52/62.31/55.25
W/o-crf-transition	80.79(±0.73)/80.96(±0.23)	68.73(±0.71)/70.35(±0.40)/66.78(±0.67)	63.89(±1.59)/62.26(±2.14)/58.67(±1.15)	40.94(±0.86)/42.72(±1.01)/40.24(±4.13)	63.59/64.08/55.23
Small-crf-transition	81.95(±0.70)/82.25(±0.39)	69.05(±0.63)/71.25(±0.76)/67.79(±1.13)	65.71(±1.68)/64.54(±1.12)/59.38(±1.20)	42.20(±1.77)/44.19(±1.22)/47.79(±0.62)	64.73/65.56/58.32
Small-emission	68.27(±4.93)/71.20(±4.40)	65.99(±1.11)/69.52(±1.53)/64.62(±2.05)	61.47(±4.16)/60.57(±2.90)/58.45(±2.78)	43.48(±1.84)/45.95(±0.64)/47.09(±1.71)	59.80/61.81/56.72
Other-classifier-init	**82.43**(±0.64)/82.18(±0.45)	69.01(±0.67)/71.66(±0.57)/67.07(±0.84)	63.70(±2.99)/63.15(±3.30)/53.61(±0.87)	42.81(±1.13)/43.95(±1.09)/27.61(±5.63)	64.49/65.24/49.43
Other-worker-init	55.15(±10.82)/54.51(±11.35)	66.53(±0.74)/68.96(±0.48)/65.42(±0.96)	62.40(±1.59)/60.68(±1.47)/53.12(±1.00)	41.57(±0.64)/45.04(±1.00)/39.96(±8.15)	56.41/57.30/52.83
Other-both-init	43.00(±13.07)/40.51(±11.60)	66.40(±1.18)/68.85(±0.97)/65.86(±1.04)	63.43(±1.26)/61.88(±1.35)/52.95(±0.81)	40.55(±0.88)/43.81(±0.89)/36.91(±8.85)	53.35/53.76/51.91
Freeze-source	79.75(±1.09)/80.63(±0.26)	67.58(±0.80)/70.29(±0.74)/67.46(±0.47)	65.70(±1.87)/65.34(±2.08)/58.03(±1.81)	44.54(±0.35)/46.19(±0.36)/47.04(±0.84)	64.39/65.61/57.51
Neural-Hidden-CRF	82.06(±0.63)/**82.28**(±0.49)	**69.16**(±0.92)/**71.89**(±0.55)/**67.99**(±0.58)	**66.87**(±1.79)/**65.55**(±1.33)/**59.69**(±0.68)	**44.94**(±0.99)/**46.61**(±0.91)/**48.44**(±0.86)	**65.76/66.58/58.71**

[1] §: "I" denotes we learn from weak supervision labels on the train data and infer the latent ground truth labels.

[2] *: "I/I" denote we learn from weak supervision labels on train/test data and infer the latent ground truth labels on the train/test data, respectively. Note that the latter three datasets are different from dataset ConLL-03 (MTurk), because they also contain weak supervision labels on the test data.

3.2.3 Equipped with Other Backbones. The deep model in our model assumes a backbone role as a feature extractor for sentence sequences. Theoretically, a more powerful deep model would be more conducive to extracting more useful contextual semantic information and delivering more accurate prediction information about the truth sequences, thus having more potential to improve the final performance. Here we conducted a small-scale study on partial datasets, where the obtained results align with the above analysis. That is, for the prediction task on datasets CoNLL-03 (WS) and WikiGold (WS), our Neural-Hidden-CRF yields suboptimal F1 performance relative to the original BERT-based one when we apply the relatively weaker deep model BiLSTM (provided by the benchmark Wrench [45])—BiLSTM-based/BERT-based: 67.63(±1.08)/69.16(±0.92), 65.21(±1.45)/66.87(±1.79). (Settings of Batch/Lr/Lr_weak/ρ: 64/0.005/0.0001/3.0, 32/0.001/0.0001/3.0.)

3.2.4 Ablation Study. Here we consider an extensive array of possible variants, involving *the ablation of different components* (variants i-iv), *the use of different parameter initialization* (variants v-vii), and *the freezing of model parameters* (variant viii). Specifically: (***i***) W/o-weak-transition: We ablate the weak source transition matrix, where we use the results inferred by the MV (Majority Voting) to represent the latent truth sequence and perform supervised learning, so that the dependencies between the truth sequence **t** and the weak label sequence **y** are not taken into account; (***ii***) W/o-crf-transition and (***iii***) Small-crf-transition[7]: We ablate/deduce the CRF transition matrix. W/o-crf-transition denotes we do not consider the CRF transition matrix at all during training and prediction/inference; Small-crf-transition denotes we proceed normally during training as usual, but use 0.5 times the value of the CRF transition matrix during prediction/inference; (***iv***) Small-emission[7]: We deduce the emission values, where we also proceed normally during training, but use 0.5 times the value of the emission values (e.g., the BERT's outputs) during prediction/inference; [8] (***v***) Other-clasifier-init: We perform the possibly inadequate learning of the parameters of the classifier part during initialization in an attempt to obtain a weaker initialization (50 back-propagations on the CoNLL-03 (MTurk) dataset and one epoch learning on the other three datasets); (***vi***) Other-worker-init: We initialize the diagonal/non-diagonal elements of the weak source transition matrix to $1/classes/0$, respectively; (***vii***)

Other-both-init: We use both of the parameter initialization ways above; (***viii***) Freeze-source: We freeze the learning of the weak source parameters in the training phase.

In Table 5, we see that: (***i***) The method shows substantial performance degradation when either the weak source transition matrix or CRF transition matrix are ablated, or emission values are attenuated; *these results directly indicate the indispensable role of all three modules* (i.e., the weak source transition matrix, the CRF transition matrix, and the emission value) and the most significant of the weak source transition matrix; (***ii***) Further, smaller emission values relative to a smaller CRF transition matrix produce a more pronounced performance degradation, illustrating the more dramatic sensitivity for emission values of our method; (***iii***) On most of the datasets, our initialization of the classifier part and the weak source part is effective; a suitable parameter initialization allows our model to achieve better performance; (***iv***) Further learning of the weak source parameters is necessary for the learning process of Neural-Hidden-CRF; (***v***) In addition, we find that the vairant Other-classifier-init outperforms Neural-Hidden-CRF in prediction on CoNLL-03 (MTurk). This is not surprising because we do not perform detailed tuning of our method, and the seemingly weaker parameter initialization happens to have stronger performance when combined with other hyperparameters.

4 CONCLUSION

This paper presents Neural-Hidden-CRF, the first neuralized undirected graphical model, for learning from weak-supervised sequence labels. Neural-Hidden-CRF embedded with a hidden CRF layer models the variables of word sequence, latent ground truth sequence, and weak label sequence, where truth sequence is provided with rich contextual semantic information by the deep learning model. Our method, therefore, benefits both from the principled modeling of graphical models and from contextual knowledge of deep learning models, while avoiding the label bias problem caused by the local optimization perspective. Our empirical evaluations on multiple benchmarks demonstrate that Neural-Hidden-CRF significantly improves state-of-the-art and provides a new solution to weakly-supervised sequence labeling.

ACKNOWLEDGMENTS

---

[7]Note that w.r.t. variants iii and iv, we investigate the performance of the variants under more ratios in the Appendix A.5.

[8]Note that it is not feasible to completely ablate emission values in the prediction, because we need to take sentence sequence **x** to predict truth sequence **t**.

REFERENCES

[1] Phil Blunsom. 2004. Hidden markov models. *Lecture notes, August* 15, 18-19 (2004), 48.

[2] Peng Cao, Yilun Xu, Yuqing Kong, and Yizhou Wang. 2019. Max-mig: an information theoretic approach for joint learning from crowds. *arXiv preprint arXiv:1905.13436* (2019).

[3] Pengpeng Chen, Hailong Sun, Yongqiang Yang, and Zhijun Chen. 2022. Adversarial Learning from Crowds. In *Proceedings of the AAAI Conference on Artificial Intelligence*, Vol. 36. 5304–5312.

[4] Zhijun Chen, Hailong Sun, Haoqian He, and Pengpeng Chen. 2023. Learning from Noisy Crowd Labels with Logics. *arXiv preprint arXiv:2302.06337* (2023).

[5] Zhijun Chen, Huimin Wang, Hailong Sun, Pengpeng Chen, Tao Han, Xudong Liu, and Jie Yang. 2020. Structured Probabilistic End-to-End Learning from Crowds.. In *IJCAI*. 1512–1518.

[6] Michael Collins. 2015. Log-linear models, memms, and crfs. *Columbia University lecture* (2015).

[7] Alexander Philip Dawid and Allan M Skene. 1979. Maximum likelihood estimation of observer error-rates using the EM algorithm. *Journal of the Royal Statistical Society: Series C (Applied Statistics)* 28, 1 (1979), 20–28.

[8] Jacob Devlin, Ming-Wei Chang, Kenton Lee, and Kristina Toutanova. 2018. Bert: Pre-training of deep bidirectional transformers for language understanding. *arXiv preprint arXiv:1810.04805* (2018).

[9] G David Forney. 1973. The viterbi algorithm. *Proc. IEEE* 61, 3 (1973), 268–278.

[10] Daniel Y. Fu, Mayee F. Chen, Frederic Sala, Sarah M. Hooper, Kayvon Fatahalian, and Christopher Ré. 2020. Fast and Three-rious: Speeding Up Weak Supervision with Triplet Methods. In *Proceedings of the 37th International Conference on Machine Learning (ICML 2020)*.

[11] Ian Goodfellow, Yoshua Bengio, Aaron Courville, and Yoshua Bengio. 2016. *Deep learning*. Vol. 1. MIT Press.

[12] Awni Hannun. 2020. The Label Bias Problem. (2020).

[13] Zhiheng Huang, Wei Xu, and Kai Yu. 2015. Bidirectional LSTM-CRF models for sequence tagging. *arXiv preprint arXiv:1508.01991* (2015).

[14] Diederik P Kingma and Jimmy Ba. 2014. Adam: A method for stochastic optimization. *arXiv preprint arXiv:1412.6980* (2014).

[15] Roman Klinger and Katrin Tomanek. 2007. *Classical probabilistic models and conditional random fields*. TU, Algorithm Engineering.

[16] John Lafferty, Andrew McCallum, and Fernando CN Pereira. 2001. Conditional random fields: Probabilistic models for segmenting and labeling sequence data. (2001).

[17] Ouyu Lan, Xiao Huang, Bill Yuchen Lin, He Jiang, Liyuan Liu, and Xiang Ren. 2019. Learning to contextually aggregate multi-source supervision for sequence labeling. *arXiv preprint arXiv:1910.04289* (2019).

[18] Yinghao Li, Pranav Shetty, Lucas Liu, Chao Zhang, and Le Song. 2021. BERTifying the Hidden Markov Model for Multi-Source Weakly Supervised Named Entity Recognition. *arXiv preprint arXiv:2105.12848* (2021).

[19] Yinghao Li, Le Song, and Chao Zhang. 2022. Sparse Conditional Hidden Markov Model for Weakly Supervised Named Entity Recognition. In *Proceedings of the 28th ACM SIGKDD Conference on Knowledge Discovery and Data Mining*. 978–988.

[20] Pierre Lison, Jeremy Barnes, and Aliaksandr Hubin. 2021. skweak: Weak Supervision Made Easy for NLP. *arXiv preprint arXiv:2104.09683* (2021).

[21] Pierre Lison, Aliaksandr Hubin, Jeremy Barnes, and Samia Touileb. 2020. Named entity recognition without labelled data: A weak supervision approach. *arXiv preprint arXiv:2004.14723* (2020).

[22] Xuezhe Ma and Eduard Hovy. 2016. End-to-end sequence labeling via bidirectional lstm-cnns-crf. *arXiv preprint arXiv:1603.01354* (2016).

[23] Kayo Matsushita, Kayo Matsushita, and Hasebe. 2018. *Deep active learning*. Springer.

[24] Andrew McCallum, Dayne Freitag, and Fernando CN Pereira. 2000. Maximum entropy Markov models for information extraction and segmentation.. In *Icml*, Vol. 17. 591–598.

[25] Todd K Moon. 1996. The expectation-maximization algorithm. *IEEE Signal processing magazine* 13, 6 (1996), 47–60.

[26] An T Nguyen, Byron C Wallace, Junyi Jessy Li, Ani Nenkova, and Matthew Lease. 2017. Aggregating and predicting sequence labels from crowd annotations. In *Proceedings of the conference. Association for Computational Linguistics. Meeting*, Vol. 2017. NIH Public Access, 299.

[27] Yassine Ouali, Céline Hudelot, and Myriam Tami. 2020. An overview of deep semi-supervised learning. *arXiv preprint arXiv:2006.05278* (2020).

[28] Alexander Ratner, Stephen H Bach, Henry Ehrenberg, Jason Fries, Sen Wu, and Christopher Ré. 2017. Snorkel: Rapid training data creation with weak supervision. In *Proceedings of the VLDB Endowment. International Conference on Very Large Data Bases*, Vol. 11. NIH Public Access, 269.

[29] Alexander Ratner, Braden Hancock, Jared Dunnmon, Frederic Sala, Shreyash Pandey, and Christopher Ré. 2019. Training complex models with multi-task weak supervision. In *Proceedings of the AAAI Conference on Artificial Intelligence*, Vol. 33. 4763–4771.

[30] Alexander J Ratner, Christopher M De Sa, Sen Wu, Daniel Selsam, and Christopher Ré. 2016. Data programming: Creating large training sets, quickly. *Advances in neural information processing systems* 29 (2016).

[31] Filipe Rodrigues, Francisco Pereira, and Bernardete Ribeiro. 2013. Learning from multiple annotators: distinguishing good from random labelers. *Pattern Recognition Letters* 34, 12 (2013), 1428–1436.

[32] Filipe Rodrigues, Francisco Pereira, and Bernardete Ribeiro. 2014. Sequence labeling with multiple annotators. *Machine learning* 95, 2 (2014), 165–181.

[33] Filipe Rodrigues and Francisco C Pereira. 2018. Deep learning from crowds. In *Thirty-Second AAAI Conference on Artificial Intelligence*.

[34] Nasim Sabetpour, Adithya Kulkarni, and Qi Li. 2020. Optsla: an optimization-based approach for sequential label aggregation. *Findings of the Association for Computational Linguistics: EMNLP 2020* (2020).

[35] Nasim Sabetpour, Adithya Kulkarni, Sihong Xie, and Qi Li. 2021. Truth discovery in sequence labels from crowds. In *2021 IEEE International Conference on Data Mining (ICDM)*. IEEE, 539–548.

[36] Esteban Safranchik, Shiying Luo, and Stephen Bach. 2020. Weakly supervised sequence tagging from noisy rules. In *Proceedings of the AAAI Conference on Artificial Intelligence*, Vol. 34. 5570–5578.

[37] Erik F Sang and Fien De Meulder. 2003. Introduction to the CoNLL-2003 shared task: Language-independent named entity recognition. *arXiv preprint cs/0306050* (2003).

[38] Gonçalo Simoes, Helena Galhardas, and Luısa Coheur. 2009. Information Extraction tasks: a survey. *Simpósio de Informática* 540 (2009), 1–550.

[39] Edwin Simpson and Iryna Gurevych. 2018. A Bayesian approach for sequence tagging with crowds. *arXiv preprint arXiv:1811.00780* (2018).

[40] Charles Sutton, Andrew McCallum, et al. 2012. An introduction to conditional random fields. *Foundations and Trends® in Machine Learning* 4, 4 (2012), 267–373.

[41] Hanna M Wallach. 2004. Conditional random fields: An introduction. *Technical Reports (CIS)* (2004), 22.

[42] Karl Weiss, Taghi M Khoshgoftaar, and DingDing Wang. 2016. A survey of transfer learning. *Journal of Big data* 3, 1 (2016), 1–40.

[43] Jing Zhang. 2022. Knowledge learning with crowdsourcing: a brief review and systematic perspective. *IEEE/CAA Journal of Automatica Sinica* 9, 5 (2022), 749–762.

[44] Jieyu Zhang, Cheng-Yu Hsieh, Yue Yu, Chao Zhang, and Alexander Ratner. 2022. A survey on programmatic weak supervision. *arXiv preprint arXiv:2202.05433* (2022).

[45] Jieyu Zhang, Yue Yu, Yinghao Li, Yujing Wang, Yaming Yang, Mao Yang, and Alexander Ratner. 2021. WRENCH: A Comprehensive Benchmark for Weak Supervision. In *Thirty-fifth Conference on Neural Information Processing Systems Datasets and Benchmarks Track (Round 2)*.

[46] Xin Zhang, Guangwei Xu, Yueheng Sun, Meishan Zhang, and Pengjun Xie. 2021. Crowdsourcing Learning as Domain Adaptation: A Case Study on Named Entity Recognition. *arXiv preprint arXiv:2105.14980* (2021).

[47] Yudian Zheng, Guoliang Li, Yuanbing Li, Caihua Shan, and Reynold Cheng. 2017. Truth inference in crowdsourcing: Is the problem solved? *Proceedings of the VLDB Endowment* 10, 5 (2017), 541–552.

A APPENDIX

A.1 Calculation of the Likelihood

First, we have the likelihood:

$$
\begin{aligned}
&\log p(\mathbf{y}^{(i)} \mid \mathbf{x}^{(i)}; \Theta) \\
&= \log \sum_{\mathbf{t}^{(i)}} p(\mathbf{y}^{(i)}, \mathbf{t}^{(i)} \mid \mathbf{x}^{(i)}; \Theta) \\
&= \log \frac{1}{Z(\mathbf{x}^{(i)}; \Theta)} \sum_{\mathbf{t}^{(i)}} \exp \left(\sum_l \sum_w \theta_w \cdot f_w(\mathbf{y}_l^{(i)}, t_{l-1}^{(i)}, t_l^{(i)}, \mathbf{x}^{(i)}, l) \right) \\
&= \log \sum_{\mathbf{t}^{(i)}} \exp \left(\sum_l \sum_w \theta_w \cdot f_w(\mathbf{y}_l^{(i)}, t_{l-1}^{(i)}, t_l^{(i)}, \mathbf{x}^{(i)}, l) \right) - \log \sum_{\mathbf{y}^{(i)}} \sum_{\mathbf{t}^{(i)}} \exp \left(\sum_l \sum_w \theta_w \cdot f_w(\mathbf{y}_l^{(i)}, t_{l-1}^{(i)}, t_l^{(i)}, \mathbf{x}^{(i)}, l) \right) \\
&= \log \sum_{\mathbf{t}^{(i)}} \exp(\Psi(\mathbf{y}^{(i)}, \mathbf{t}^{(i)}, \mathbf{x}^{(i)})) - \log \sum_{\mathbf{y}^{(i)}} \sum_{\mathbf{t}^{(i)}} \exp(\Psi(\mathbf{y}^{(i)}, \mathbf{t}^{(i)}, \mathbf{x}^{(i)})),
\end{aligned}
\tag{A.1}
$$

where we use $\Psi(\mathbf{y}^{(i)}, \mathbf{t}^{(i)}, \mathbf{x}^{(i)})$ to implement the abbreviation. We present the detail calculations of $\log \sum_{\mathbf{t}^{(i)}} \exp(\Psi(\mathbf{y}^{(i)}, \mathbf{t}^{(i)}, \mathbf{x}^{(i)}))$ and $\log \sum_{\mathbf{y}^{(i)}} \sum_{\mathbf{t}^{(i)}} \exp(\Psi(\mathbf{y}^{(i)}, \mathbf{t}^{(i)}, \mathbf{x}^{(i)}))$ in the following.

A.1.1 Calculation of $\log \sum_{\mathbf{t}^{(i)}} \exp(\Psi(\mathbf{y}^{(i)}, \mathbf{t}^{(i)}, \mathbf{x}^{(i)}))$. First, we define $\boldsymbol{\alpha}_{l,k}^{(i)} \triangleq \log \left[\sum_{\mathbf{t}_{1\sim l}^{(i)}} \exp(\Psi(\mathbf{y}_{1\sim l}^{(i)}, \mathbf{t}_{1\sim l-1}^{(i)}, t_l^{(i)} = k, \mathbf{x}_{1\sim l}^{(i)})) \right]$, which is used to express the logarithm of the cumulative sum of the scores after the exponential operation for each path that satisfies "the state of $\mathbf{t}^{(i)}$ at time step l is k"; here the path is considered only from the beginning to the time step l.

Then, we have:

$$
\begin{aligned}
&\log \left[\sum_{\mathbf{t}^{(i)}} \exp(\Psi(\mathbf{y}^{(i)}, \mathbf{t}^{(i)}, \mathbf{x}^{(i)})) \right] \\
&= \log \left[\sum_{\mathbf{t}_{1\sim L}^{(i)}} \exp(\Psi(\mathbf{y}_{1\sim L}^{(i)}, \mathbf{t}_{1\sim L}^{(i)}, \mathbf{x}_{1\sim L}^{(i)})) \right] \\
&= \log \left[\sum_{k=1}^{K} \sum_{\mathbf{t}_{1\sim L-1}^{(i)}} \exp(\Psi(\mathbf{y}_{1\sim L}^{(i)}, \mathbf{t}_{1\sim L}^{(i)}, t_L = k, \mathbf{x}_{1\sim L}^{(i)})) \right] \\
&= \log \left[\sum_{k=1}^{K} \exp(\boldsymbol{\alpha}_{L-1,k}^{(i)}) \right].
\end{aligned}
\tag{A.2}
$$

Thus, we transform the original objective of calculating $\log \sum_{\mathbf{t}^{(i)}} \exp(\Psi(\mathbf{y}^{(i)}, \mathbf{t}^{(i)}, \mathbf{x}^{(i)}))$ into the calculating the "log_sum_exp" (i.e., the successive operations of $\exp(\cdot)$, cumulative calculation and $\log(\cdot)$) of vector $\boldsymbol{\alpha}_{L-1,:}^{(i)}$.

Now we use dynamic programming to calculate $\boldsymbol{\alpha}^{(i)}$. The recursive calculation of $\boldsymbol{\alpha}^{(i)}$ is as follows:

$$
\begin{aligned}
\boldsymbol{\alpha}_{l,k}^{(i)} &\triangleq \log \left[\sum_{\mathbf{t}_{1\sim l-1}^{(i)}} \exp(\Psi(\mathbf{y}_{1\sim l}^{(i)}, \mathbf{t}_{1\sim l-1}^{(i)}, t_l = k, \mathbf{x}_{1\sim l}^{(i)})) \right] \\
&= \log \left[\sum_{k'=1}^{K} \sum_{\mathbf{t}_{1\sim l-2}} \exp \left(\Psi(\mathbf{y}_{1\sim l-1}^{(i)}, \mathbf{t}_{1\sim l-2}^{(i)}, t_{l-1}^{(i)} = k', \mathbf{x}_{1\sim l-1}^{(i)}) + E_{k,l}^{(i)} + T_{k',k} + W_{k,\mathbf{y}_l^{(i)}} \right) \right] \\
&= \log \left[\sum_{k'=1}^{K} \exp(\boldsymbol{\alpha}_{l-1,k'}^{(i)} + E_{k,l}^{(i)} + T_{k',k} + W_{k,\mathbf{y}_l^{(i)}}) \right],
\end{aligned}
\tag{A.3}
$$

where $W_{k,\mathbf{y}_l^{(i)}} = \sum_{j \in \mathcal{J}^{(i)}} \pi_{k,y_l^{(i,j)}}^{(j)}$, and $E_{k,l}^{(i)}$, $T_{k',k}$, $W_{k,\mathbf{y}_l^{(i)}}$ denote the *emission score*, the *CRF transition score*, and the *weak source transition score*, which originate from the three kind of feature functions.

The boundary case of $\boldsymbol{\alpha}^{(i)}$ is:

$$
\boldsymbol{\alpha}_{0,k}^{(i)} = \begin{cases} \underbrace{0}_{\text{obtained from } \log(1)} & \text{if } k = \text{BEGIN} \\ \underbrace{-10000}_{\text{replace } \log(0) = -\infty} & \text{otherwise.} \end{cases}
\tag{A.4}
$$

A.1.2 Calculation of $\log \sum_{\mathbf{y}^{(i)}} \sum_{\mathbf{t}^{(i)}} \exp(\Psi(\mathbf{y}^{(i)}, \mathbf{t}^{(i)}, \mathbf{x}^{(i)}))$. First, we define $\boldsymbol{\beta}_{l,k}^{(i)} \triangleq \log \left[\sum_{\mathbf{y}_{1\sim l}^{(i)}} \sum_{\mathbf{t}_{1\sim l-1}^{(i)}} \exp(\Psi(\mathbf{y}_{1\sim l}^{(i)}, \mathbf{t}_{1\sim l-1}^{(i)}, t_l^{(i)} = k, \mathbf{x}_{1\sim l}^{(i)})) \right]$.

Similar to the derivation in Equation A.2, we can do the following derivation for $\log \sum_{\mathbf{y}^{(i)}} \sum_{\mathbf{t}^{(i)}} \exp(\Psi(\mathbf{y}^{(i)}, \mathbf{t}^{(i)}, \mathbf{x}^{(i)}))$.

Thus, we have:

$$
\begin{aligned}
&\log \left[\sum_{\mathbf{y}^{(i)}} \sum_{\mathbf{t}^{(i)}} \exp(\Psi(\mathbf{y}^{(i)}, \mathbf{t}^{(i)}, \mathbf{x}^{(i)})) \right] \\
&= \log \left[\sum_{\mathbf{y}_{1\sim L}^{(i)}} \sum_{\mathbf{t}_{1\sim L}^{(i)}} \exp(\Psi(\mathbf{y}_{1\sim L}^{(i)}, \mathbf{t}_{1\sim L}^{(i)}, \mathbf{x}_{1\sim L}^{(i)})) \right] \\
&= \log \left[\sum_{k=1}^{K} \sum_{\mathbf{y}_{1\sim L}^{(i)}} \sum_{\mathbf{t}_{1\sim L-1}^{(i)}} \exp(\Psi(\mathbf{y}_{1\sim L}^{(i)}, \mathbf{t}_{1\sim L}^{(i)}, t_L^{(i)} = k, \mathbf{x}_{1\sim L}^{(i)})) \right] \\
&= \log \left[\sum_{k=1}^{K} \exp(\boldsymbol{\beta}_{L-1,k}^{(i)}) \right].
\end{aligned}
\tag{A.5}
$$

The recursive calculation of $\boldsymbol{\beta}^{(i)}$ is:

$$
\begin{aligned}
\boldsymbol{\beta}_{l,k}^{(i)} &\triangleq \log \left[\sum_{\mathbf{y}_{1\sim l}^{(i)}} \sum_{\mathbf{t}_{1\sim l-1}^{(i)}} \exp(\Psi(\mathbf{y}_{1\sim l}^{(i)}, \mathbf{t}_{1\sim l-1}^{(i)}, t_l^{(i)} = k, \mathbf{x}_{1\sim l}^{(i)})) \right] \\
&= \log \left[\sum_{k'=1}^{K} \sum_{\mathbf{y}_{1\sim l-1}^{(i)}} \sum_{\mathbf{t}_{1\sim l-2}^{(i)}} \sum_{\mathbf{y}_l^{(i)}} \exp \left(\Psi(\mathbf{y}_{1\sim l-1}^{(i)}, \mathbf{t}_{1\sim l-2}^{(i)}, t_{l-1}^{(i)} = k', \mathbf{x}_{1\sim l-1}^{(i)}) + E_{k,l}^{(i)} + T_{k',k} + W_{k,\mathbf{y}_l^{(i)}} \right) \right] \\
&= \log \left[\sum_{k=1}^{K} \sum_{\mathbf{y}_{1\sim l-1}^{(i)}} \sum_{\mathbf{t}_{1\sim l-2}^{(i)}} \exp \left(\Psi(\mathbf{y}_{1\sim l-1}^{(i)}, \mathbf{t}_{1\sim l-2}^{(i)}, t_{l-1}^{(i)} = k', \mathbf{x}_{1\sim l-1}^{(i)}) + E_{k,l}^{(i)} + T_{k',k} + \log \sum_{\mathbf{y}_l^{(i)}} \exp(W_{k,\mathbf{y}_l^{(i)}}) \right) \right] \\
&= \log \left[\sum_{k'=1}^{K} \exp \left(\boldsymbol{\beta}_{l-1,k'}^{(i)} + E_{k,l}^{(i)} + T_{k',k} + \log \sum_{\mathbf{y}_l^{(i)}} \exp(W_{k,\mathbf{y}_l^{(i)}}) \right) \right],
\end{aligned}
\tag{A.6}
$$

where the meanings of $E_{k,l}^{(i)}, T_{k',k}, W_{k,\mathbf{y}_l^{(i)}}$ are the same as those of the corresponding symbols in Equation A.3. Also, the boundary case is:

$$
\boldsymbol{\beta}_{0,k}^{(i)} = \begin{cases} \underbrace{0}_{\text{obtained from } \log(1)} & \text{if } k = \text{BEGIN} \\ \underbrace{-10000}_{\text{replace } \log(0) = -\infty} & \text{otherwise.} \end{cases}
\tag{A.7}
$$

Specifically, in Equation A.6, we can also use dynamic programming to calculate $\log \sum_{\mathbf{y}_l^{(i)}} \exp(W_{k,\mathbf{y}_l^{(i)}})$.

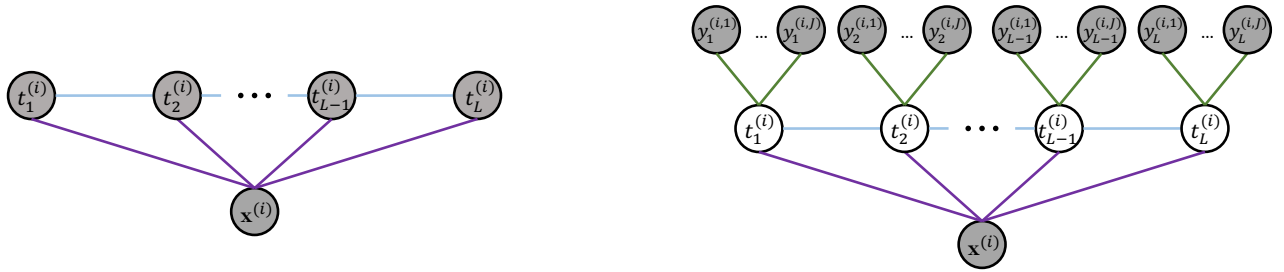## A.2 Probabilistic Graphical Representation

Figure A.1: Probabilistic graphical representation of CRF (left) vs. Neural-Hidden-CRF (right).

A.3 Experimental Configurations

Table A.1: Configurations on CoNLL-03 (MTurk).

	Batch§	Lr*	Lr_weak†	$\rho^\dagger$
MV + BiLSTM-CRF	32	0.1	-	-
MV + BiLSTM	1	0.01	-	-
CL (VW)	32	0.1	-	-
CL (VW-B)	128	0.001	-	-
CL (MW)	32	0.1	-	-
Neural-Hidden-CRF	64	0.1	0.0001	2.0
Gold + BiLSTM-CRF	1	0.01	-	-

1 $\S$: The search space of batch size is: (1, 32, 64, 128).
2 $*$: The search space of learning rate is: (0.1, 0.01, 0.001).
3 $\dagger$: The search spaces for our specific hyper-parameters are: Lr_weak: (0.001, 0.0001), ρ: (2.0).

Table A.2: Configurations of Neural-Hidden-CRF on CoNLL-03 (WS), WikiGold (WS) and MIT-Restaurant (WS).

	Batch§	Lr§	Lr_crf§	Lr_weak*	ρ^*
Conll (P)	32	2e-5	0.001	0.001	2.0
Conll (I)	32	2e-5	0.01	0.001	2.0
Wikigold (P)	16	2e-5	0.005	0.001	2.0
Wikigold (I)	32	3e-5	0.001	0.001	2.0
Mit-Rest. (P)	32	2e-5	0.001	0.01	6.0
Mit-Rest. (I)	16	2e-5	0.01	0.2	5.0

1 $\S$: The search spaces are consistent with benchmark [45].
2 $*$: The search spaces for our specific hyper-parameters on Mit-Rest are: Lr_weak=(0.2,0.1,0.01), ρ=(5.0, 6.0). On other datasets, our model more easily yields satisfactory results, and we always set them (0.001, 2.0).

A.4 Suggestions for Setting Hyperparameters

When applying our Neural-Hidden-CRF to other datasets, in most cases, we recommend considering the following suggestions for setting hyperparameters.

- For Batch (batch size): Our suggested finding space is {8, 16, 32, 64, ...}, and batch size should not be set to 1 (which would not be conducive to the challenging multi-source weak supervision learning context);
- For Lr_weak (learning rate of weak source transition matrix): We suggest that Lr_weak be set equal to or less than the learning rate of the CRF layer (i.e., Lr_crf);
- For ρ (in Equation 21): Our suggested finding space is {2.0, 3.0, 4.0, 5.0, 6.0} for most cases;
- For the pre-train of the classifier part of the model (mentioned in Section 2.5): We suggest using better super-parameters (e.g., batch size, learning rates, etc.) for pre-training to get a better parameter initialization.

A.5 Performance of More Variants
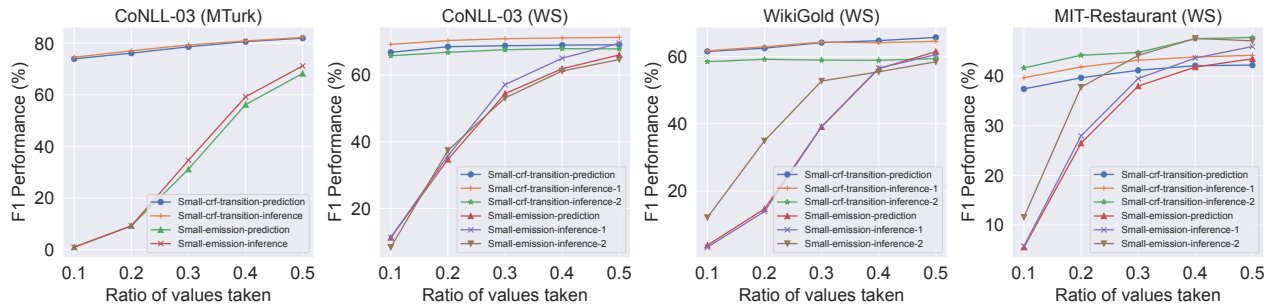
Figure A.2: Performance of more variants for supplementary ablation study. Results are averaged over 20 runs.